Gold-gold luminosity increase in RHIC for a beam energy scan with colliding beam energies extending below the nominal injection energy

C. Liu,* P. Adams, E. Beebe, S. Binello, I. Blackler, M. Blaskiewicz, D. Bruno, B. Coe, K. A. Brown, K. A. Drees, A. V. Fedotov, W. Fischer, C. J. Gardner, C. Giorgio, X. Gu, T. Hayes, H. Huang, R. Hulsart, T. Kanesue, D. Kayran, N. Kling, B. Lepore, Y. Luo, D. Maffei, G. Marr, A. Marusic, K. Mernick, R. Michnoff, M. Minty, J. Morris, C. Naylor, S. Nemesure, M. Okamura, I. Pinayev, S. Polizzo, D. Raparia, G. Robert-Demolaize, T. Roser, J. Sandberg, V. Schoefer, S. Seletskiy, F. Severino, T. Shrey, P. Thieberger, M. Valette, A. Zaltsman, K. Zeno, I. Zane, W. Zhang, and H. Zhao

Brookhaven National Laboratory, Upton, New York 11973, USA

(Received 11 November 2021; accepted 8 April 2022; published 5 May 2022)

The Beam Energy Scan phase II (BES-II), performed in the Relativistic Heavy Ion Collider (RHIC) from 2019 to 2021, explored the phase transition between quark-gluon plasma and hadronic gas. BES-II exceeded the goal of a fourfold increase in the average luminosity over that achieved during Beam Energy Scan phase I (BES-I), at five gold beam energies: 9.8, 7.3, 5.75, 4.59, and 3.85 GeV/nucleon. This was accomplished by addressing several beam dynamics effects, including intrabeam scattering, beam-beam, space charge, beam instability, and field errors induced by superconducting magnet persistent currents. Some of these effects are especially detrimental at low energies. BES-II achievements are presented, and the measures taken to improve RHIC performance are described. These measures span the whole RHIC complex, including ion beam sources, injectors, beam lifetime improvements in RHIC, and operation with the world's first bunched beam Low Energy RHIC electron Cooler (LEReC).

DOI: 10.1103/PhysRevAccelBeams.25.051001

I. INTRODUCTION

The quantum chromodynamics (QCD) phase diagram [1] has evolved into a more complex diagram with theoretical and experimental progress but still has uncharted territories. In particular, the nature of the transformation from the quark-gluon plasma to the state of hadronic gas is unknown [2]. The questions are, for example, whether the QCD phase diagram has a first order phase transition, whether there is a QCD critical point [3,4], and whether there is a critical end point where the phase transition is of second order.

To demonstrate the existence and establish the location of the critical point is a major goal of several heavy ion experiments. These include the NA49 and NA61/SHINE [5] experiments at the CERN SPS, Beam Energy Scans I and II (BES-I/II) [6–8] at the Relativistic Heavy Ion Collider (RHIC) [9], and future programs at the Facility for Anti-proton and Ion Research (FAIR) [10,11] at GSI and the Nuclotron-based Ion Collider Facility (NICA) at JINR [12].

BES-I and BES-II explored the structure of the phase diagram by taking gold beam collision data at five energies: 9.8, 7.3, 5.75, 4.59, and 3.85 GeV/nucleon. BES-I operated from 2007 to 2014 at various energies for short periods of time, in order to provide preliminary data for the experiments, and to study the various beam dynamics effects that limit machine performance.

A plan for major hardware upgrades was put in place at the end of BES-I, including for example electron cooling and 9 MHz rf cavities. These upgrades were used during BES-II from 2019 to 2021 at descending beam energies, with well-defined physics goals at each energy. The main goal was to provide enough experimental data by increasing the average luminosity by a factor of 4. This goal was achieved, and in some cases exceeded, in part by improving the initial luminosity at the beginning of a store and by increasing the luminosity lifetime. The electron cooling system was used at the two lowest beam energies (4.59 and 3.85 GeV/nucleon). The luminosities achieved in BES-I and BES-II are presented in Fig. 1, and the primary beam parameters are summarized in Table I.

The beam energy scans were challenging because the energies are well below the nominal energy range in RHIC—at or below gold beam injection energy of

*cliu1@bnl.gov

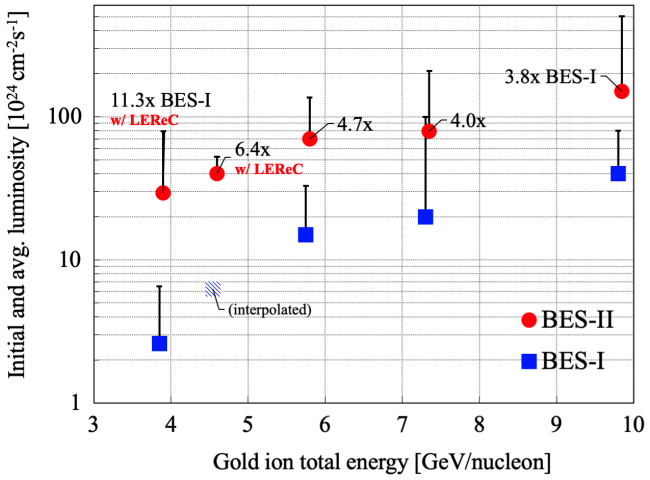

FIG. 1. The initial and average luminosities at five gold beam energies achieved during BES-I and BES-II. Red dots and blue squares represent the average luminosity. A small horizontal bar marks the initial luminosity. The average luminosity at 4.59 GeV/nucleon during BES-I is interpolated based on data collected at 3.85 and 5.75 GeV/nucleon.

9.8 GeV/nucleon. In contrast to routine RHIC operations beams were injected directly into collision at each energy—there was no energy ramp, removal of beam separations, or β-squeeze before collisions. Only in the middle of stores with electron cooling did a β-squeeze take place, in order to benefit from the reduced beam emittance.

Several physical effects [13–15] and other adverse operational conditions limit the beam lifetime. All become more challenging at lower energies. The most significant ones are intrabeam scattering (IBS), space charge, beam-beam, beam instability, and persistent current effects. Table II in Sec. III shows how lower energies enhance IBS growth rates. The space charge tune shift increases quadratically with a decreasing beam energy [see Eq. (5) in Sec. IV]. Even though the beam-beam parameter is energy independent when assuming constant normalized transverse emittances [see Eq. (6) in Sec. IV], low energy beams are more susceptible to beam-beam driven resonances. Persistent current effects in superconducting magnets are stronger at the low currents used for low energy beams (see Sec. VI). The rf bucket acceptance diminishes with lower beam energy (see Fig. 19), limiting their bunch intensity

TABLE I. Beam parameters for BES-I and BES-II at various energies.

		9.8 GeV/nucleon		7.3 GeV/nucleon		5.75 GeV/nucleon		4.59 GeV/nucleon		3.85 GeV/nucleon	
Parameters	(Units)	BES-I	BES-II	BES-I	BES-II	BES-I	BES-II	BES-I	BES-II	BES-I	BES-II
Bunch intensity N[a]	(10^9)	0.9	1.8	1.1	1.75	1.1	1.7	0.4	1.1	0.5	1.5
β^*	(m)	2.5	2	3.5	3	6	4	10	4.5	6	4.5
Fractional tune		0.23	0.09	0.23	0.09	0.23	0.12	0.23	0.23	0.23	0.23/0.12
Chromaticity[b]		NA	−10	NA	−8	NA	−7	NA	−6	NA	−5
rms emittance $\epsilon_{x,y}$	(μm)	2.5	1.8	1.7	2.2	2.5	2.1	1.5	1.5	1.7	1.5
Bunch length σ_s	(m)	1.6	1.4	1.8	2.2	1.4	1.5	1.4	3.5	1.6	12[c]
Harmonics		360	360	360	360	360	363/121	366	120	369	123/369
rf frequency[d]	(MHz)	28	28	28	28	28	28/9	28	9	28	9/28
Bucket area	(eV s)	0.9	0.9	0.54	0.54	0.36	0.481	0.25	0.81	0.18	0.6
Longitudinal emittance	(eV s)	0.7	0.82	0.5	0.5		0.28		0.5		0.24
Beam-beam parameter	(10^{-3})	2.1	4.1	1.7	3.4	2.1	3.4	0.076	3.8	0.095	3.5
SC tune shift		0.013	0.05	0.036	0.07	0.058	0.11	0.01	0.09	0.036	0.1
Cooling		No	No	No	No	No	No	No	Yes	No	Yes
Demagnetization		No	Yes	No	Yes	No	Yes	No	Yes	No	Yes
Store length	(min)	35	60	45	45	20	23	15	40	10	25
Average luminosity L_{ave} $10^{24}\text{cm}^{-2}\text{s}^{-1}$		40	150	20	79	15	70	6.25[e]	40	2.6	29.4
Improved factor		3.8		4.0		4.7		6.4		11.3	

[a]The bunch intensity was measured at the start of physics data taking, which is lower than the injected bunch intensity (Fig. 18). In all cases there were 111 bunches.
[b]BES-I chromaticities were difficult to measure and control, before the demagnetization cycle was devised.
[c]This bunch length is the full width at half maximum of the flattened longitudinal profile.
[d]In the 28/9 and 9/28 cases of a double rf system, the first value is the primary rf frequency.
[e]This average luminosity is interpolated from those achieved at 5.75 and 3.85 GeV/nucleon.

capacity. The finite resolution of dipole corrector settings [16] also becomes an issue at low beam energies.

We elaborate below on the challenges that were encountered and on the countermeasures that were taken to improve the initial luminosity within the vertex cut (Sec. II) and the luminosity lifetime. Section [17] discusses the IBS effect and countermeasures—LEReC cooling and the double rf scheme. Section IV presents space charge countermeasures and the interplay between space charge and beam-beam effects. Section V discusses the beam instability issue and the bunch-by-bunch feedback system. Section VI details how demagnetization cycles alleviate persistent current effects. Section VII describes the minimization of the β-function at the collision point (β^*). Section VIII focuses on the injector setup optimizations that improve the bunch intensity. Section IX lists other improvements that are indispensable in improving the average luminosity.

II. LUMINOSITY WITHIN THE VERTEX CUT

The luminosity of a symmetric collider like RHIC is

$$L = \frac{N^2 H f_{\text{rep}}}{4\pi\sigma_x\sigma_y}, \tag{1}$$

where N is the number of particles in a bunch, σ_x and σ_y are the rms beam sizes in the horizontal and vertical planes, H is a geometric factor that accounts for the crossing angle, beam offsets at the collision point and the hourglass effect, and f_{rep} is the bunch repetition rate. The beam energy scans had neither a crossing angle nor a beam offset, and so H reduces to the hourglass factor

$$H = \sqrt{\pi}\, A\, \exp(A^2)\, \text{erfc}(A), \tag{2}$$

where

$$A = \frac{\beta^*}{\sigma_s}, \tag{3}$$

β^* is the β-function at the collision point, σ_s is the rms bunch length, and $\text{erfc}(A)$ is the complementary error function. With $H \approx 1$ for BES-I/II collisions, the luminosity does not depend on the bunch length.

The central part of the experimental detector has a beryllium beam pipe and a limited longitudinal acceptance. It is desirable to suppress the background due to secondary particles that have hadronic interactions in the aluminum beam pipe further from the interaction point (IP). For both of these reasons a vertex cut is applied to limit the selection of events to those that occur within ± 70 cm of the IP. Events originating in the range from ± 70 to ± 150 cm are only counted with a 30% efficiency factor. The vertex cut causes the usable luminosity to depend on the bunch length; effective luminosity decreases with increasing bunch length.

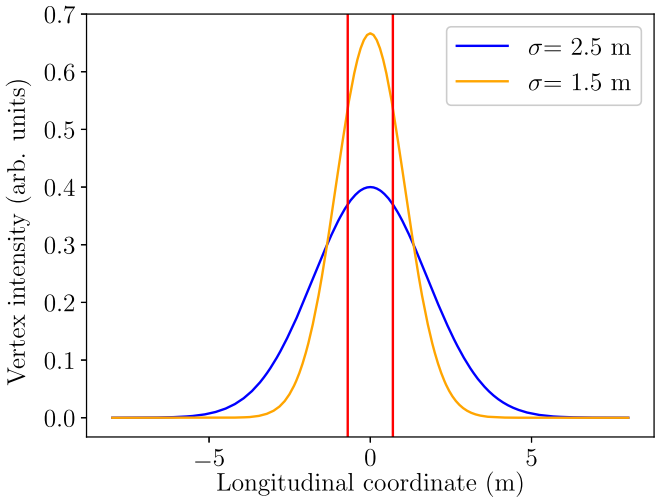

FIG. 2. The longitudinal vertex distribution for a long bunch ($\sigma_s = 2.5$ m) with the lower frequency cavities (9 MHz) and a short bunch ($\sigma_s = 1.5$ m) with the higher frequency cavities (28 MHz). The red vertical lines indicate the vertex cut range of ± 0.7 m about the detector center. This cut reduces the instantaneous luminosity by ~70% and ~50% for long and short bunches, respectively.

Figure 2 shows the longitudinal distribution of collision events (the vertex distribution) for two different rf systems: one with 9 MHz cavities creating longer bunches, the other with 28 MHz cavities [18] creating shorter bunches. The event rate in the central part of the detector (marked by the red vertical lines) is about 40% higher for the shorter bunches than for the longer bunches. However, a lower peak current alleviates space charge and beam instability effects and provides a better event resolution in the detector. These factors were evaluated at each collision energy to choose the optimum single or double rf system.

III. COUNTERACTING INTRABEAM SCATTERING

Intrabeam scattering (IBS) [17,19] occurs when charged particles within a single bunch scatter off each other through Coulomb interactions. This dilutes the longitudinal phase space density. The presence of betatron coupling and dispersion causes all three bunch sizes to increase over time. The rate of beam quality deterioration is characterized by three IBS growth rates, for the transverse beam sizes and the momentum spread

$$\frac{1}{T_p} = \frac{1}{\sigma_p}\frac{d\sigma_p}{dt}, \quad \frac{1}{T_x} = \frac{1}{\epsilon_x^{1/2}}\frac{d\epsilon_x^{1/2}}{dt}, \quad \frac{1}{T_y} = \frac{1}{\epsilon_y^{1/2}}\frac{d\epsilon_y^{1/2}}{dt}, \tag{4}$$

where σ_p is the momentum spread, and ϵ_x and ϵ_y are the horizontal and vertical emittances. IBS strongly limited the

TABLE II. Simulated longitudinal and horizontal IBS growth times for beam sizes at BES-I/II beam energies for the cases with the 28 MHz cavities and 9 MHz cavities. The differences in bunch intensity N at the same energies are due to the expected differences in longitudinal acceptance of the two rf systems.

	28 MHz cavities			9 MHz cavities		
Energy (GeV/nucleon)	$N(10^9)$	T_p (min)	T_x (min)	$N(10^9)$	T_p (min)	T_x (min)
3.85	0.5	18	43	0.6	20	117
4.59	0.5	28	63	0.8	19	134
5.75	1.1	14	28	1.3	20	131
7.3	1.8	33	49	2.1	14	142
9.8	2.1	56	77	2.3	15	150

luminosity lifetime during the BES-I runs and remained a major challenge for BES-II operation. Growth times at BES-I/II beam energies range from 10 min to 10's of min, as shown in Table II for results calculated using BETACOOL [20].

The IBS growth of gold ion beams in the BES-II runs was counteracted by cooling the gold ions with electrons. LEReC, the Low Energy RHIC electron Cooling [21] facility at RHIC, was proposed and built as the world's first bunched electron beam cooling device. Commissioned in 2018 and 2019, cooling was made available for operation at the two lowest beam energies [22]. IBS effects were less severe at the other energies, and their cooling was not in the LEReC scope. Electron cooling [23–25] reduced the energy spread and therefore also the bunch length, as well as the transverse beam emittances. It enabled the average luminosity to increase by 60% to 100%, compared to collisions without cooling [26].

Electron cooling was not available at 5.75 GeV/nucleon. A double rf system was implemented instead, using 9 MHz cavities in addition to the primary 28 MHz cavities. IBS growth rates [27,28] were reduced as a result of the larger bucket area and the stronger longitudinal focusing. This is discussed further in Sec. III C.

A. The Low Energy RHIC electron Cooler

LEReC, shown Fig. 3, is an rf-accelerated bunched electron beam cooler with a laser-driven photoinjector [29]. It combats IBS growth at the two lowest beam energies by cooling the ion beams in collision, improving the average luminosities. The electron bunches that are generated by the 400 kV dc electron photocathode gun pass through rf acceleration and various stages of gymnastics to obtain a very low energy spread of about 2×10^{-4}. Each electron macrobunch consists of 30 to 36 electron bunches at a 704 MHz repetition frequency. The 0.4 nsec long bunches overlap with a single ion bunch with a 9 MHz repetition rate, as shown in Fig. 4. The electron beam first copropagates at the same velocity as the ion beam in the Yellow ring and then turns around to copropagate with the ion beam in the Blue ring. Thanks to its small relative energy spread and small angular divergence, the electron beam reduces (cools) the ion beam divergence via Coulomb interactions.

B. Optimizing RHIC during electron cooling

Three-dimensional electron cooling of colliding beams in both RHIC rings was realized for the first time [22] during BES-II. Longitudinal cooling was observed in the bunch length measurements made by the wall current monitor [30]. Transverse cooling was monitored by the transverse profiles measured by the H-jet fluorescence image system [31]. Figure 5 shows the evolution of the ion beam emittance, with and without electron cooling, at an energy of 3.85 GeV/nucleon. Reducing the bunch length enhanced the proportion of collisions in the range of the vertex cut. Transverse cooling increased the luminosity significantly by shrinking the transverse emittances and enabling a reduction of the β function at the interaction point, which would otherwise not be possible due to limited aperture at the final focusing quadrupoles.

Figure 6 shows collision rates with and without cooling. The store length with cooling was increased by about

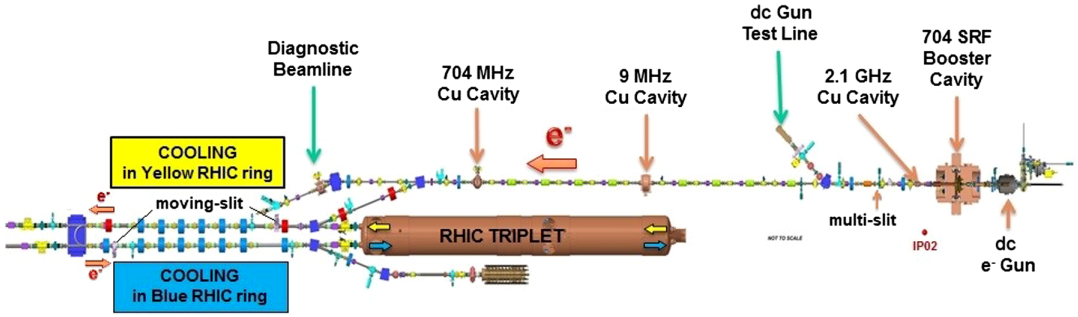

FIG. 3. Schematic of the Low Energy RHIC electron Cooling accelerator. Electron beam is accelerated by a 704 MHz superconducting rf cavity to the required energy and then transported to the RHIC cooling sections. First they merge with ion bunches in the Yellow ring cooling section, before turning around and merging with ion bunches in the Blue RHIC ring. Finally they are transported to a beam dump.

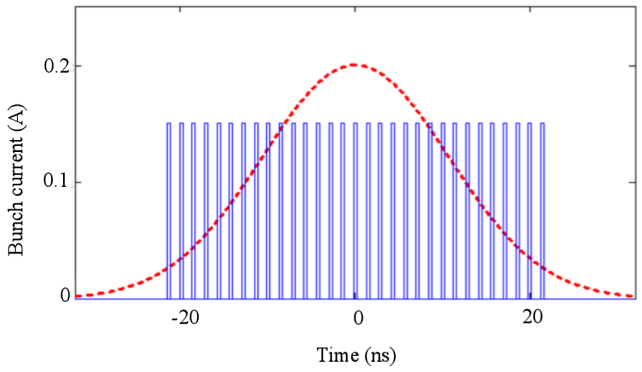

FIG. 4. The LEReC electron beam and RHIC ion beam time structure, showing the overlap of 30 to 36 electron bunches (blue) with a single gold ion bunch (red). The electron bunches are spaced by 1.4 nsec (704 MHz), with a charge of 0.13 nC and a length of 0.4 nsec. The gold ion bunch has a charge of 7.5 nC and a bunch repetition frequency of 9 MHz.

10 to 40 min, thanks to the improved luminosity lifetime. The β^* at 3.85 GeV/nucleon was squeezed from 4.5 to 3 m when the beam emittance was cooled by about 30%, leading to a further significant luminosity increase. The squeeze was not performed at the beginning of a store, because the initially large beam emittances would have caused unacceptable beam losses. Nonetheless the squeeze was performed as early as possible, to maximize the benefit before losing too much beam intensity. The final β^* value was determined according to the maximum permissible beam size in the final focusing quadrupoles and the transverse emittance at the time of the squeeze.

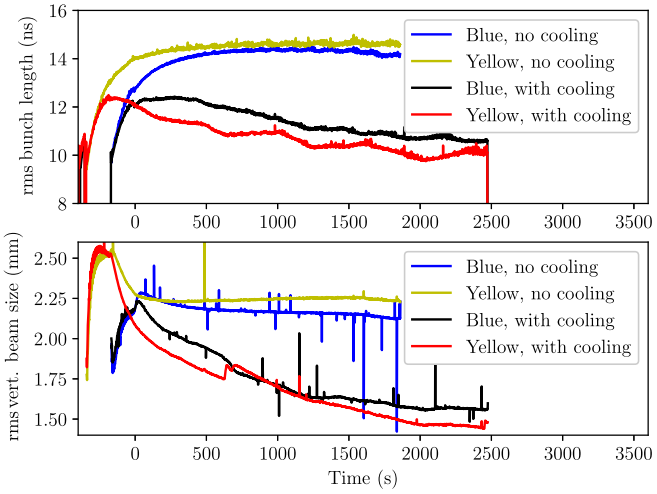

FIG. 5. Ion beam emittance evolution, with and without electron cooling. Upper plot: rms bunch length. Lower plot: vertical beam size. The blue and yellow traces are without cooling, while the black and red traces are with cooling. The Yellow beam was injected about 3 min before the Blue beam. The time origin marks the start of physics data taking, soon after both rings were filled.

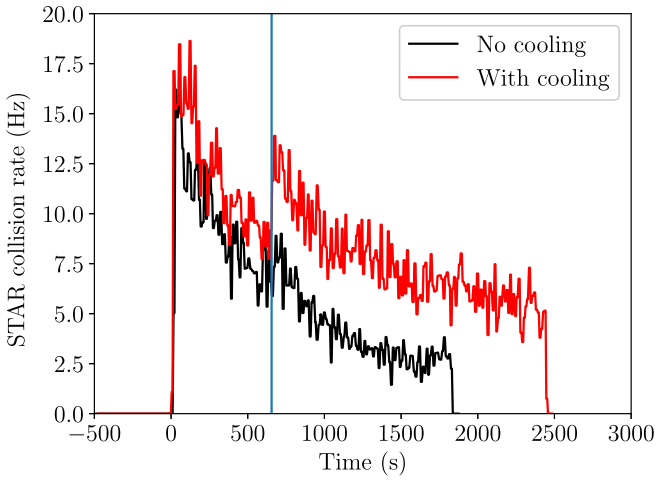

FIG. 6. Collision rates during stores at 3.85 GeV/nucleon, with (red trace) and without (black trace) cooling. The store length with cooling was usually about 10 min longer. The vertical line indicates the time when the β function at the collision point was squeezed, with cooling.

Optimizing stores with cooling is a multidimensional iterative process that includes tuning both the electron beam quality [29,32,33] and also ion beam parameters. Here we focus on the parameters that have the most profound effect on cooling efficiency and on ion beam lifetime.

The cooling section gold beam β functions were scanned in the range from 25 to 100 m in an effort to improve the cooling efficiency by reducing the angular spread of the ion beams. The electron beam size was always adjusted to match the size of the ion beam. Electron-induced ion emittance growth and beam losses [34] dominated at the largest β functions, probably due to space charge interactions. As a compromise, the ion beam β function was empirically set to about 25 m, corresponding to an rms beam size of about 3.5 mm. A study of the heating effect was begun, and is still ongoing after the completion of BES-II, to close the gap between experimental data and theoretical prediction.

Tune space scans, near the integer, below 0.25 and also just below the half-integer found that electron cooling efficiency was the best with ion beam fractional betatron tunes [35] of about 0.23.

A significant effort was spent on improving cooling by optimizing electron beam parameters [29,32,33], especially the beam current and the energy spread, and on optimizing the 3D matching between the electron and ion beams. The electron beam current was scanned to optimize the store average luminosity, balancing the effects of electron beam heating and cooling. Optimal cooling was reached with an electron current of 15–20 mA at 4.59 GeV/nucleon and 14–18 mA at 3.85 GeV/nucleon, in both cases with a fractional tune of 0.23.

Early operations at 3.85 GeV/nucleon were performed with fractional tunes at 0.23. Tune space was explored

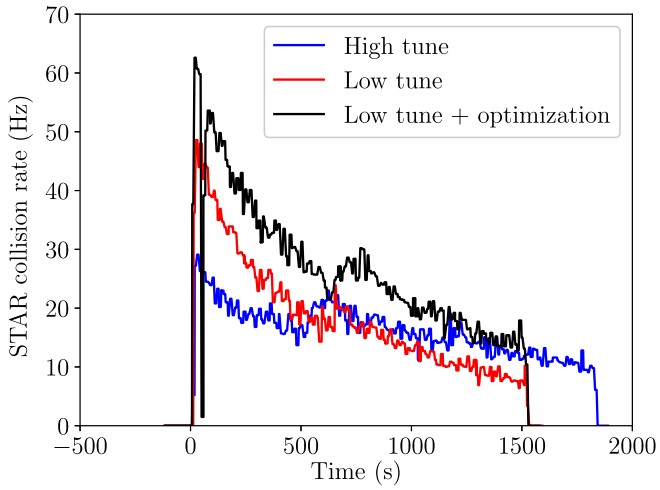

FIG. 7. The experimental collision rates for stores at 3.85 GeV/nucleon with different fractional betatron tunes. The blue data were taken with fractional tunes of 0.23, when the electron cooling efficiency was higher. The red data correspond to fractional tunes of 0.12, when the cooling efficiency was reduced but the ion beam lifetime was increased. The black data were taken after fine betatron tune adjustments and with smaller electron beam currents, further improving the ion beam lifetime with less heating.

again, this time with the goal of optimizing the average luminosity rather than enhancing just the cooling efficiency, and in particular to find better betatron tunes that enhance the ion beam lifetime in the presence of the high-current electron beam. Performance at 3.85 GeV/nucleon improved significantly when the fractional betatron tunes were lowered from 0.23 to 0.12. The single beam lifetime and the beam lifetime in collision were both improved, the injected bunch intensity was increased, and the initial collision rate was boosted by a factor of 2.

Section IV discusses how maximizing the ion beam lifetime in collisions leads to fractional tunes around 0.1, depending on the space charge tune shift. These lower tunes reduced the transverse and longitudinal cooling rates, compared to fractional tunes at 0.23, because lower electron beam currents are required to maintain acceptable ion beam lifetimes. The average luminosity was comparable at the lower fractional tune, even though the luminosity lifetime suffered due to ion interactions with the electron beam. The electron beam current was then rescanned, greatly alleviating the electron-induced ion-beam losses and increasing the average luminosity beyond the best achieved with the high fractional tune. Additional fine-tuning of the betatron tunes of both ion beams increased the average luminosity even further, exceeding the best high fractional tune value by about 50%, as shown in Fig. 7.

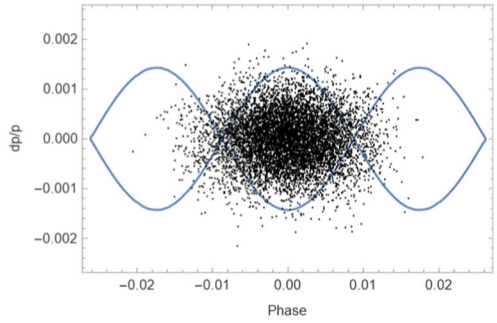

(a) Initial distribution with a single RF system

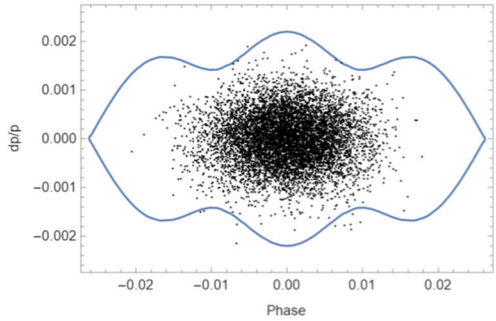

(b) Initial distribution with a double RF system

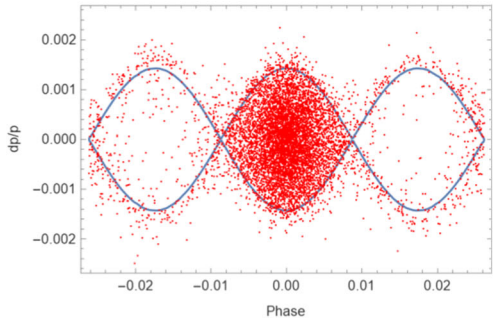

(c) Distribution after 7000 turns, single RF system

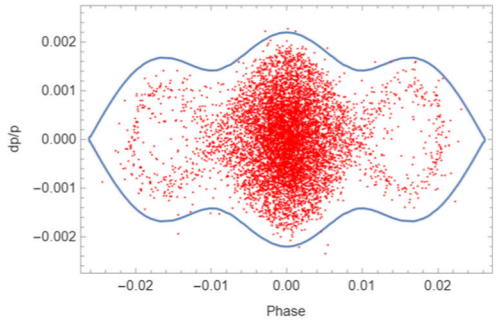

(d) Distribution after 7000 turns, double RF system

FIG. 8. Longitudinal phase space distribution for a single rf system (28 MHz) and a double rf system (28 and 9 MHz), before and after 7000 turns. The double rf system (b) provides a larger central bucket area than the single rf system (a). Debunched beam after 7000 turns is negligible in the double rf case (d), compared to the single rf case (c).

TABLE III. Longitudinal emittances and bunch intensities at AGS extraction for the five BES-II energies. The "Merge scheme" column records the rf gymnastics bunch merging scheme used in the AGS to increase the number of particles per bunch. The longitudinal "Emittance" is the 95% emittance, 6 times the rms emittance. The maximum number of bunches that could be extracted during each AGS cycle varied from 2 to 4.

Beam energy E (GeV/nucleon)	Source	Merge scheme	Emittance (eV s)	Bunch intensity (10^9)	Maximum number of bunches
9.8	EBIS	12-2	0.817	2.66	2
7.3	EBIS	12-2	0.693	2.5	2
5.75	Tandem	8-4	0.28	2.3	4
4.59	EBIS	12-3	0.53	2.66	3
3.85	Tandem	8-4	0.2	2.3	4

C. Reducing IBS growth rates with a second rf system

The bucket acceptance of a single 28 MHz system with a total voltage of 400 kV was originally 0.367 eVs/nucleon at 5.75 GeV/nucleon. Bunches arriving from alternating gradient synchrotron (AGS) have a longitudinal emittance of about 0.7 eVs/nucleon, due to the 12-to-2 bunch merge used for beam from electron beam ion source (EBIS) [36]. Figures 8 and 19 show how this small bucket acceptance significantly limits the RHIC beam captured efficiency.

This prompted two changes. The first was to use the Tandem [37] ion source to provide bunches with lower longitudinal emittance (see Table III), still with adequate intensity at 5.75 GeV/nucleon. The second change was to increase the bucket acceptance by engaging the 9 MHz rf system with a total voltage of 180 kV at the same synchronous phase as the 28 MHz system. This increased the central bucket area from 0.367 eVs/nucleon to 0.481 eVs/nucleon, as shown in Fig. 8. A further benefit is that IBS growth rates are reduced and the bunched beam lifetime is increased when the second rf system is added, as shown in Fig. 9.

The RHIC abort gap is formed by not filling 9 of the 120 buckets that are available, providing time for the leading edge of the abort kicker pulse. Debunched heavy ion beam reaching the abort gap is usually cleaned in routine operations, enabling clean aborts. Simulation [38] suggests that debunched beam is almost negligible with the double rf system, as shown in Fig. 8. In fact it is not necessary to clean the abort gap at 5.75 GeV/nucleon, unlike operations at 9.8 and 7.3 GeV/nucleon.

IV. ALLEVIATING THE SPACE CHARGE EFFECT

The space charge effect [39] also limits the beam lifetime at the BES-I/II energies. The space charge tune shift increases approximately like $1/\gamma^3$ at lower beam energies [39], since

$$\delta Q_{x,y} = \frac{r_0 N}{2\pi\epsilon_{x,y}\beta^2\gamma^3} = \frac{r_0 N}{2\pi\epsilon^n_{x,y}\beta\gamma^2}, \tag{5}$$

where $r_0 = q^2/mc^2$ is the classical electrostatic radius of the particle, N is the bunch intensity, $\epsilon_{x,y}$ and $\epsilon^n_{x,y}$ are the geometric and normalized transverse beam emittances, and β is the relative velocity. Figure 10 shows that the space charge tune shift was larger in BES-II than in BES-I, because the bunch intensity was much larger, as shown in Fig. 18.

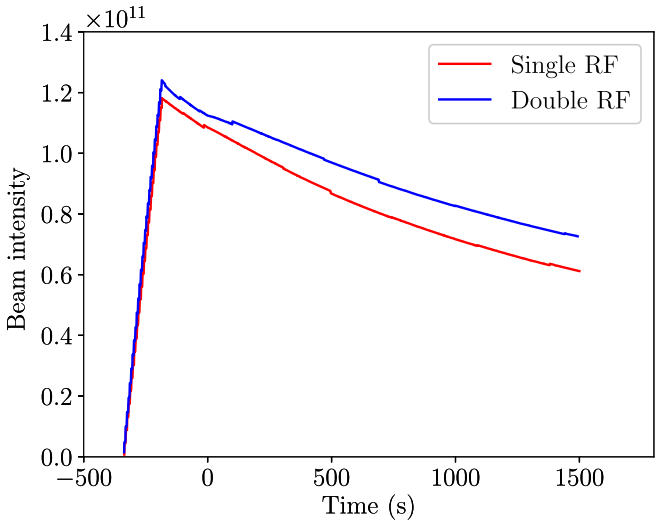

FIG. 9. Evolution of the bunched beam intensity with a single rf system (red trace) and with a double rf system (blue trace).

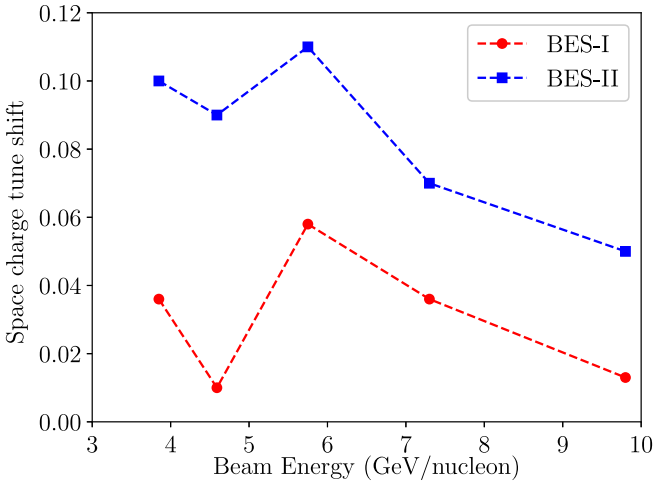

FIG. 10. Incoherent space charge tune shift in BES-I and BES-II at various beam energies. The lines connecting the data points are for the purpose of guiding the viewer's eye and have no physical meaning.

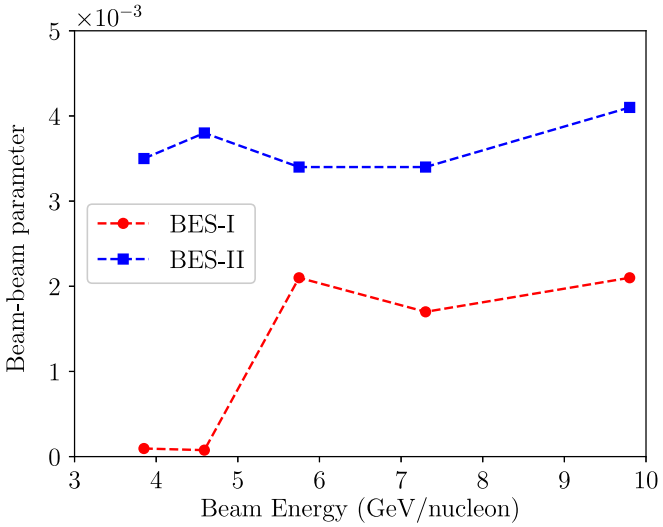

FIG. 11. Beam-beam parameters in BES-I and BES-II at various beam energies.

A. Selecting the betatron tune to alleviate space charge and beam-beam effects

The beam-beam parameter for a round beam is

$$\xi = \frac{N r_0 \beta^*}{4\pi\gamma\sigma^2}, \tag{6}$$

where

$$\sigma = \sqrt{\frac{\beta^* \epsilon^n}{\beta\gamma}} \tag{7}$$

is the transverse rms beam size, with BES-I and BES-II values shown in Fig. 11. The beam-beam force drives resonances that can hurt the beam lifetime, even though the BES beam-beam parameters were much smaller than the RHIC value of about 0.015 at top energy [40]. The fractional tunes were carefully selected and operationally tested during BES-II, alleviating both space charge and beam-beam effects.

The beam lifetime improved when some low order resonances (5, 6, and so on) were avoided by moving the fractional tune closer to the integer, consistent with the simulation results [40]. For example, the tunes were lowered from 0.23 to 0.09 at 9.8 and 7.3 GeV/nucleon. The fractional tunes at 5.75 GeV/nucleon evolved during the 2020 run, as discussed further below. Although the fractional tunes were initially chosen to be 0.23 for higher cooling efficiency at 4.59 and 3.85 GeV/nucleon, later they were moved to 0.12 at 3.85 GeV/nucleon, as discussed in Sec. III B.

Bunch intensities increased more and more during 5.75 GeV/nucleon operations when the second rf system was employed, eventually raising the space charge tune shift from the design value of 0.06 to over 0.10, as shown in Fig. 10. This moved the tune of the beam core down, close to the integer resonance, especially when the fractional tune was 0.09. Beam emittance blowup was observed during beam filling, leading to severe degradation of the initial luminosity. In consequence the betatron tunes were later increased to 0.12, moving the beam core tunes away from the integer. The emittances measured at tunes of 0.09 and 0.12 are shown in Fig. 12.

Raising the fractional tunes from 0.09 to 0.12 not only avoided emittance blowup but also enabled RHIC to accept higher bunch intensities from the injector, thanks to the increased AGS intensity limit. It became routine to lower the fractional tune slightly as the intensity diminished, from an initial value of about 0.122 at the beginning of a store.

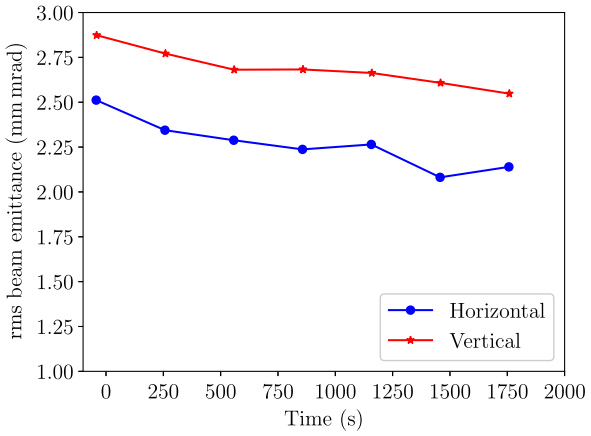

(a) With a fractional tune of 0.09

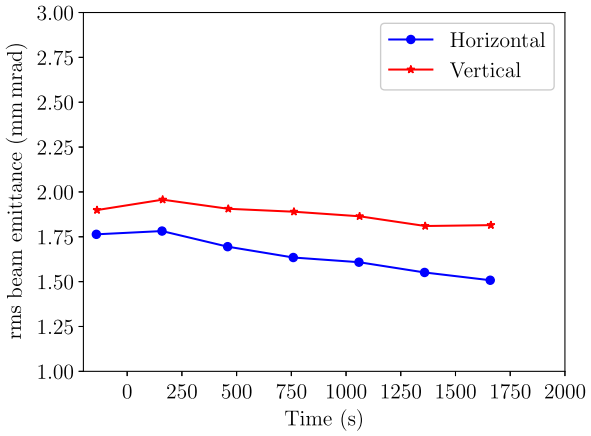

(b) With a fractional tune of 0.12

FIG. 12. Transverse emittance blowup due to the space charge effect. A 50% increase was observed with the fractional part of betatron tunes at 0.09 (a) compared to the emittance with the fractional part of betatron tunes later raised to 0.12 (b). The blowup can be seen in the initial values comparing the left and right plots. The horizontal emittance is shown in blue and the vertical emittance is shown in red. The vertical emittance was reported to be higher than the horizontal likely due to the calibration of measurement devices.

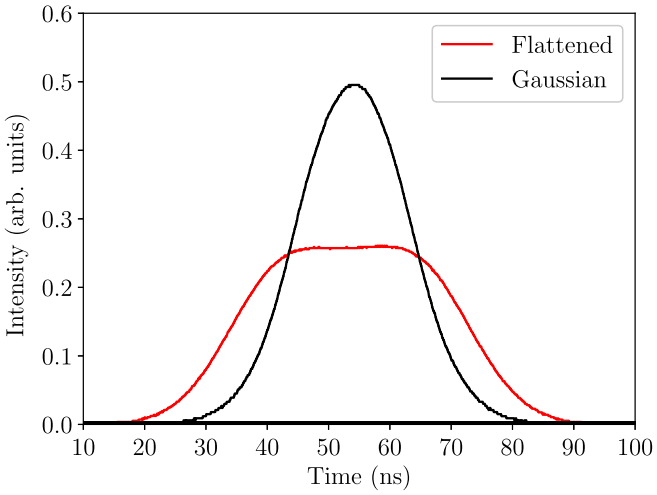

FIG. 13. Gaussian longitudinal profile (the black curve) for a single rf system and flattened longitudinal profile (the red curve) for a double rf system, with the third harmonic cavities phased opposite to the primary rf.

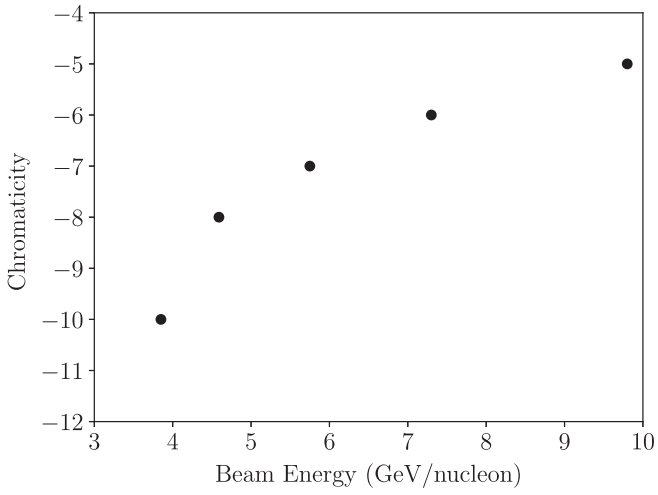

FIG. 14. Nominal chromaticity settings at various energies during BES-II, required to suppress the coupled bunch instability.

These measures, taken together, increased the average luminosity by more than 50% when compared to the average with fractional tunes of 0.09.

B. Reducing the peak current with third harmonic cavities

Reducing the peak current is a well-known way to alleviate space charge effects [41]. However, during BES-I/II it came with the side effect of reducing the fraction of collisions within the vertex cut. Nonetheless the luminosity increased significantly when this technique was applied at 3.85 GeV/nucleon, because it enabled collisions with much higher bunch intensities.

Figure 13 shows how the bunch profile was flattened when third harmonic cavities (28 MHz, 60 kV) were employed in addition to the fundamental rf system (9 MHz, 180 kV). Fast beam loss at injection without the third harmonic was observed with 1.6×10^9 injected bunch intensity, caused by a space charge tune shift of up to 0.14. RHIC was able to maintain 60% higher initial bunch intensities when fast losses were eliminated by bunch flattening. The benefits of higher bunch intensities and better lifetimes overcame the drawback of lower vertex cut efficiencies. The initial luminosity improved by a factor of 2 and the average luminosity improved by more than a factor of 2.

V. BEAM INSTABILITY AND BUNCH-BY-BUNCH FEEDBACK

The coupled bunch instability has been a common issue in RHIC at all energies and for all species [42,43]. The issue was more pronounced in BES-II than in BES-I because the bunch intensity was pushed considerably higher, as shown in Fig. 18. Figure 14 shows how more negative chromaticity was required to provide more Landau damping at lower beam energies below the transition energy (23.5 GeV/nucleon) in order to stay below the instability threshold [44,45]. This is in common with routine practice in RHIC.

Raising the absolute chromaticity increases the tune spread. On one hand, this suppresses beam instability. On the other hand, it leads to shorter beam lifetime, because the beam experiences more resonances. An attempt was made to reduce the contribution of amplitude dependent detuning to the total tune spread by using octupoles [46,47]. Both means of reducing the total tune footprint—by lowering chromaticities and by adjusting octupoles—consistently resulted in beam instability. The goal of operating with a smaller tune spread for better lifetime made it necessary to enhance beam stability with a bunch-by-bunch transverse feedback system.

A. The bunch-by-bunch feedback system

The bunch-by-bunch feedback system that was implemented and commissioned for operation at 3.85 GeV/nucleon kicks each bunch independently, and so damps all coupled bunch modes of coherent oscillations. This system upgraded a previous system that worked successfully, but which was not used in routine operations. The new system used the same stripline kickers and rf amplifiers to drive the kickers, while the electronics and firmware that implement the damping algorithm [48] and generate the kicker waveform were modified. New beam position monitor (BPM) variable-gain analog front ends and signal processing firmware were developed. This signal processing allowed low noise, single turn, accurate single bunch position measurements, even with the relatively weak BPM signals that are due to the longer bunches and lower bunch charges characteristic of BES-II running.

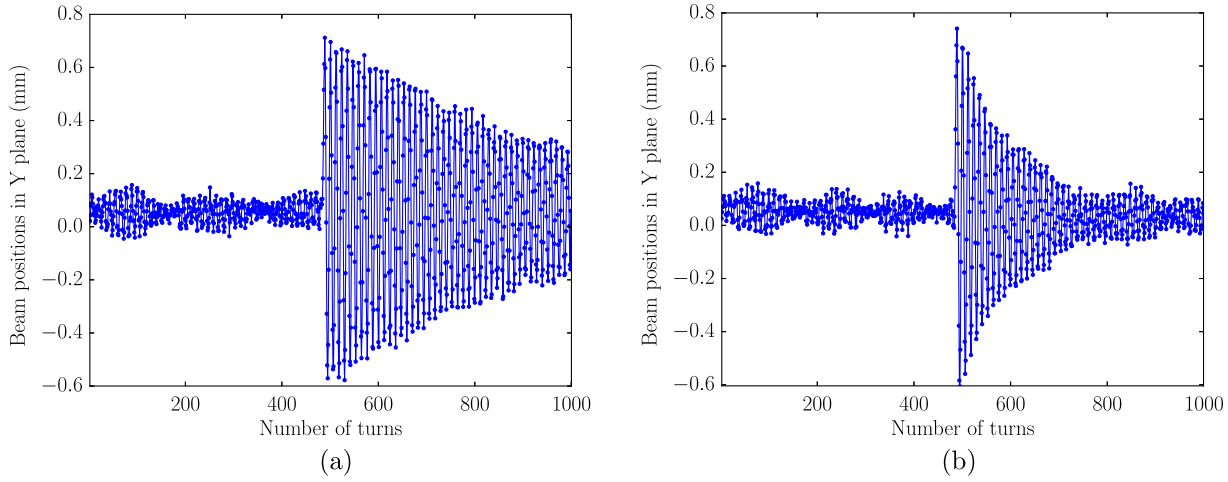

FIG. 15. Suppressing turn-by-turn orbit oscillations with the bunch-by-bunch damper in a test. The oscillation begins at turn 512 when the tune meter kicker excites the beam. (a) Without damper (b) With damper.

B. Operational experience of the bunch-by-bunch feedback system

The system was tested by damping oscillations driven by the RHIC tune meter kicker. Figure 15 shows the response of the beam with and without the system engaged, after the tune meter kicker excited a turn-by-turn oscillation on turn 512. For testing purposes the absolute value of the chromaticity was reduced, in order to slow down the natural signal decoherence.

Two benefits emerged from operating at 3.85 GeV/nucleon with both the bunch-by-bunch damper and also the double rf system [49]. First, the beam instability was suppressed, minimizing the probability of losing stores and improving operational reliability. Second, the injected bunch intensity increased by as much as 10% and the luminosity increased by as much as 20% because beam emittance dilution was suppressed. Beam dilution with the feedback system off was a result of injecting beams directly into collision. Injection oscillations in one ring disturbed the stored beam in the other ring through the beam-beam effect and enlarged the emittance. The reflection of the injection kicker pulse also excited a few bunches in the injected beam. Both of these disturbances were alleviated when bunch-by-bunch feedback was turned on.

VI. DEMAGNETIZING SUPERCONDUCTING MAGNETS TO ALLEVIATE PERSISTENT CURRENTS

Persistent currents, which alter the transport current distribution within superconducting filaments [50], have long been observed to cause operational challenges in superconducting colliders [51–54]. Persistent current effects in the RHIC superconducting dipole magnets were especially strong when operating at the low BES-I/II energies. This was evident in bench measurements of the sextupole component in the dipoles during up and down ramps, with strong hysteresis [55].

Persistent currents in RHIC dipoles produce excessive field errors at low currents. Due to the sextupole component dominated field errors, during BES-I the linear chromaticity was so difficult to control that it required reversing the polarity of sextupole families [55]. The persistent currents–induced field errors strongly limited the beam lifetime at low energies.

Persistent currents decay with time, usually with timescales from 10's of minutes to hours. This initially resulted in unstable machine conditions during BES-I. Fast changes in the beam orbit, tunes, and chromaticities were observed after changes in the operating state of the main dipoles. Long wait times were necessary to allow the persistent currents to settle whenever operations at a certain dipole current were re-established. Machine conditions were necessarily interrupted and restored frequently during BES-II operations—typically once every day or two—in order to accommodate other programs such as LEReC development and coherent electron cooling [56,57] commissioning. For high energy operation of RHIC or other colliders, the persistent current effects were detrimental only when beam was sitting at the injection energy. But these effects stay with the beam during BES-I/II because beams were injected at collision energies which were below the nominal injection energy. For all of these reasons it was beneficial to suppress the persistent currents in the main dipoles.

A demagnetization cycle [58] was introduced in which the main dipole current oscillated a few times with a diminishing amplitude before settling at the nominal operating current, as shown in Fig. 16(b). After the demagnetization cycle the dipoles were in a state that was equally sensitive to small increments and decrements of the superimposed fields, canceling persistent effects to a

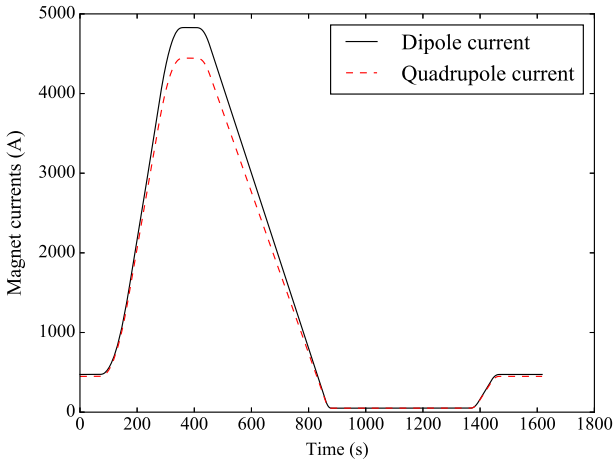

(a) Conventional magnetic cycle

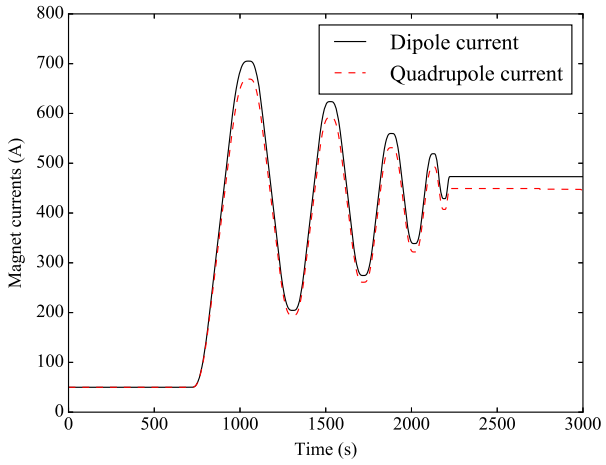

(b) Demagnetization cycle

FIG. 16. The conventional magnetic cycle (a) and the demagnetization cycle (b) for beam operations at an RHIC main dipole current of 473 A. The demagnetization cycle removed a large fraction of the persistent current. Similar demagnetization cycles were implemented at all other BES-II energies.

large extent, and thereby reducing the field errors and their time dependency.

Demagnetization cycles were implemented for all energies at and below the injection energy during BES-II operation. Beam measurements after the demagnetization cycle [58] confirmed that persistent current effects—especially sextupole field errors—were substantially reduced. Measured chromaticities were in a good agreement with model predictions with the sextupole component in the dipoles removed. Beam lifetime benefited with sextupole errors and field decay largely eliminated. Equally important, demagnetization cycles facilitated quick and frequent transitions between different operating modes.

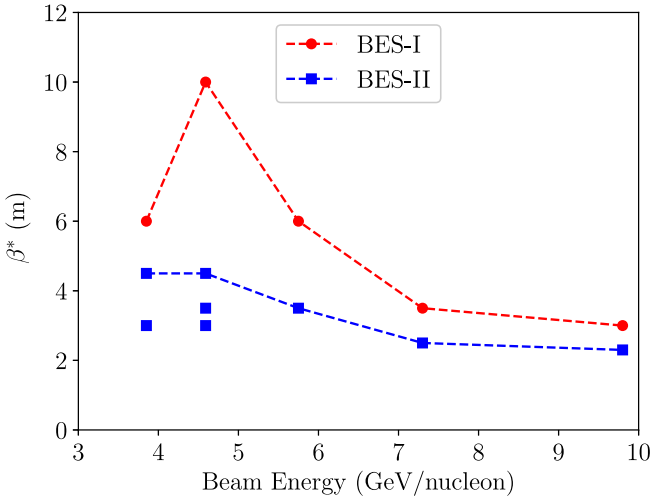

FIG. 17. Initial β^* values were smaller during BES-II than during BES-I, at all beam energies. The β^* values were reduced even more during stores with electron cooling: once at 3.85 GeV/nucleon and twice at 4.59 GeV/nucleon.

VII. MINIMIZING β^*

β-function values at interaction point IP6 were reduced for all five energies during BES-II, compared to those used for BES-I, thanks to reduced field errors and improved machine stability—see Fig. 17. This increased the luminosity further, limited by the aperture of the final focusing quadrupoles near IP6. The β^* values at the two lowest energies were further squeezed in the middle of BES-II stores after the beam emittances were sufficiently reduced by electron cooling to ensure enough aperture in the final focusing quadrupoles. Such a dynamic β-squeeze [59] was performed twice within 4.59 GeV/nucleon stores, thanks to the relatively high cooling efficiency at that energy.

VIII. INJECTOR SETUP AND BUNCH INTENSITY

Bunch intensities were significantly larger during BES-II than during BES-I (Fig. 18). These increases were enabled by beam lifetime improvements in RHIC and by injector setup improvements. Beam intensity increases at the two lowest energies were due to reduced space charge effects achieved through lower peak currents, enabled by using rf cavities with a lower frequency during BES-II (9 MHz) than during BES-I (28 MHz). In addition, the bucket acceptances at these two lowest energies were significantly larger in BES-II, as shown in Fig. 19.

The rf system settings selected at individual BES-II energies were based on considerations of space charge, IBS, and luminosity reduction due to the vertex cut. Only the higher frequency 28 MHz cavities were used for the three higher beam energies, because (i) the beam lifetimes at the maximum bunch intensity available from the injectors were reasonable (see Table III), (ii) IBS growth rates with stronger longitudinal focusing from the 28 MHz cavities were smaller, and (iii) a larger fraction of the

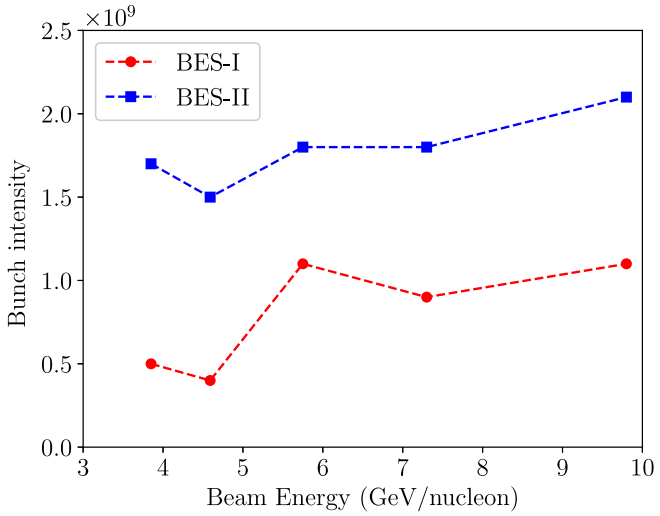

FIG. 18. The bunch intensity during BES-I and BES-II at various beam energies.

beam population was inside the vertex cut (see Fig. 2), increasing the effective luminosity by about a factor of 2. The lower frequency 9 MHz cavities were used at the two lowest energies, in order to reduce the space charge effect and therefore accommodate the higher bunch intensities provided by the injectors. Quantitative comparisons favored the 28 MHz cavities at a beam energy of 7.3 GeV/nucleon [60].

Extensive beam setup and tuning took place in the injectors [61,62], in order to provide the beam intensities and qualities required by BES-II. Both front end sources—the electron beam ion source (EBIS) [36] and the Tandem [37]—provide a wide range of ion species, including the gold beam used in the BES-I/II programs.

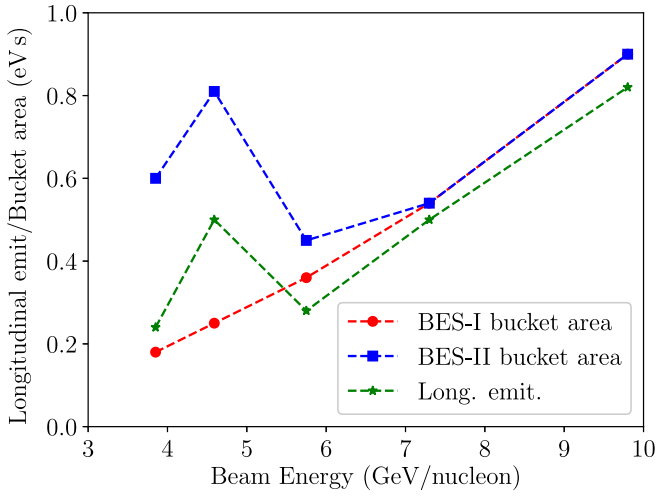

FIG. 19. The bucket acceptances achieved by the rf systems during BES-I and BES-II and the longitudinal emittance of bunches coming out of the AGS during BES-II.

Gold beam was provided by EBIS at all but two beam energies, 3.85 and 5.75 GeV/nucleon, for which the Tandem preinjector was used. At 3.85 GeV/nucleon the Tandem provided twice as many bunches of the desired intensity per injector cycle. This was critical for achieving the shortest filling time. At 5.75 GeV/nucleon the RHIC bucket acceptance was limited, making it preferable to use the smaller longitudinal emittances available from the Tandem. Table III [62] shows the AGS extracted beam parameters used during BES-II operations. Frequent rotations of the stripping foils [63] in the injector chain were necessary because of their relatively rapid deterioration, due to the significantly higher beam intensities per cycle [61].

IX. OTHER IMPROVEMENTS

Two other changes made during BES-II operations also contributed to significant average luminosity increases. The orbit correction controller was upgraded from 12 to 16 bits, sharpening orbit control to a precision of better than 50 μm. The injection kicker [64] termination was optimized to achieve a shorter rise time and a longer flattop [65], enabling longer bunches to be injected from the AGS into 9 MHz RHIC buckets and also reducing emittance dilution by providing a smoother flattop.

X. SUMMARY

The 3-year Beam Energy Scan phase II operation at RHIC was successfully completed in 2021. Average luminosities at all energies achieved or exceeded the goal of a fourfold increase over those achieved in phase I. This success was realized by implementing several measures that increased the initial bunch intensity, and the beam and luminosity lifetimes.

Intrabeam scattering growth rates were mitigated by Low Energy RHIC electron Cooling at the two lowest energies, 3.85 and 4.59 GeV/nucleon. The luminosity improved by 60% to 100% after cooling was optimized by tuning the electron and ion beam parameters. A secondary rf system provided a larger bucket area and stronger longitudinal focusing, further reducing emittance dilution due to IBS at 5.75 GeV/nucleon.

Space charge and beam-beam impacts on the beam lifetime were ameliorated by lowering the fractional tunes to around 0.1 at 9.8, 7.3, and 5.75 GeV/nucleon. This enabled the tune footprint to avoid as many strong resonances as possible.

Low frequency 9 MHz cavities were used at 4.59 and 3.85 GeV/nucleon, enabling lower peak currents and weakening the space charge effect. Third harmonic 28 MHz cavities were also used at 3.85 GeV/nucleon, to further reduce the peak currents. An equally large benefit of low frequency operation was the increased bucket acceptance, which was critical for accepting larger

intensities from the injectors. Although the effective luminosity ratio (after a vertex cut) was lower at lower rf frequencies, this shortcoming was overcome by the higher bunch intensities.

A bunch-by-bunch transverse damper system was commissioned and implemented in operation at 3.85 GeV/nucleon. This eliminated beam instabilities and improved the injected bunch brightness by combating emittance dilution during the injection process.

Demagnetization cycles were used at all BES-II energies to reduce persistent current–induced sextupolar and higher order field errors in the arc dipoles and also the drift of the magnetic field. This not only improved beam lifetimes but also facilitated quick and frequent transitions between multiple programs and studies at different energies.

The β^* values were reduced at all energies, compared to BES-I. Dynamic reductions were possible midstore at the two lowest energies, once ion emittances were sufficiently reduced by electron cooling.

The newer EBIS with modern controls provided gold beam under most circumstances. The Tandem improved RHIC performance at two beam energies. At 5.75 GeV/nucleon the Tandem provided a smaller longitudinal emittance, better matched to the limited RHIC acceptance. At 3.85 GeV/nucleon it provided more extracted bunches (four) to shorten the filling time.

A. Energy-by-energy

9.8 GeV/nucleon.—Fractional tunes less than 0.1 gave better lifetimes in the presence of space charge and beam-beam effects. Demagnetization cycles alleviated persistent current effects. Used 28 MHz rf only to increase the fraction of events within the vertex cut. Smaller β^*. Higher bunch intensities.

7.3 GeV/nucleon.—Fractional tunes less than 0.1. Demagnetization cycle. Used 28 MHz rf only. Smaller β^*. Higher bunch intensities.

5.75 GeV/nucleon.—Raised fractional tunes just above 0.1 to accommodate enhanced space charge and beam-beam tune shifts. Demagnetization cycle. Used 28 MHz primary and 9 MHz secondary rf to increase the bucket areas and strengthen longitudinal focusing. Smaller β^*. Higher bunch intensities. Smaller longitudinal emittance beam from the Tandem.

4.59 GeV/nucleon.—Electron cooling on. Fractional tunes at 0.23 gave higher cooling efficiency. Used 9 MHz rf only to increase bucket areas and to reduce peak currents, weakening space charge effects. Demagnetization cycle. Smaller initial β^*. Dynamic β^*-squeezes after sufficient cooling. Higher bunch intensities.

3.85 GeV/nucleon.—Electron cooling on. Fractional tunes lowered from 0.23 to 0.12 for luminosity optimization. Electron beam current scan. Used 9 MHz primary and 28 MHz secondary rf to flatten the bunch profile and weaken the space charge effect. Demagnetization cycle. Smaller initial β^*. Dynamic β^*-squeeze. Higher bunch intensities and short filling times with four bunches from the Tandem.

[1] N. Cabibbo and G. Parisi, Exponential hadronic spectrum and quark liberation, Phys. Lett. **59B**, 67 (1975).

[2] M. Stephanov, QCD phase diagram and the critical point, Int. J. Mod. Phys. A **20**, 4387 (2005).

[3] M. Stephanov, K. Rajagopal, and E. Shuryak, Signatures of the Tricritical Point in QCD, Phys. Rev. Lett. **81**, 4816 (1998).

[4] G. Stephans, critRHIC: The RHIC low energy program, J. Phys. G. **32**, S447 (2006).

[5] M. Gadzicki, Onset of deconfinement and critical point: NA49 and NA61/SHINE at the CERN SPS, Eur. Phys. J. Spec. Top. **155**, 37 (2008).

[6] C. Yang, The STAR beam energy scan phase II physics and upgrades, Nucl. Phys. **A967**, 800 (2017).

[7] C. Montag *et al.*, Experience with low-energy gold-gold operations in RHIC during FY 2010, Brookhaven National Laboratory, Upton, NY, Report No. BNL-99580-2013-TECH, 2013.

[8] C. Liu *et al.*, Improving the luminosity for Beam Energy Scan II at RHIC, in *Proceedings of the 10th International Particle Accelerator Conference, IPAC-2019, Melbourne, Australia, 2019* (JACoW Publishing, Geneva, Switzerland, 2019), pp. 540–543.

[9] M. Harrison, S. Peggs, and T. Roser, The RHIC accelerator, Annu. Rev. Nucl. Part. Sci. **52**, 425 (2002).

[10] M. Durante *et al.*, All the fun of the FAIR: Fundamental physics at the facility for antiproton and ion research, arXiv:1903.05693.

[11] P. Spiller, Challenges and progress in the FAIR Accelerator Project, in *Proceedings of the 21st Particle Accelerator Conference, Knoxville, TN, 2005* (IEEE, Piscataway, NJ, 2005).

[12] I. N. Meshkov, Project of the Nuclotron-based Ion Collider Facility (NICA) and multipurpose detector (MPD) at JINR, Int. J. Mod. Phys. E **18**, 438 (2009).

[13] T. Satogata *et al.*, RHIC challenges for low energy operation, in *Proceedings of the 22nd Particle Accelerator Conference, PAC-2007, Albuquerque, NM* (IEEE, New York, 2007), pp. 1877–1879.

[14] A. V. Fedotov *et al.*, Beam dynamics limits for low-energy RHIC operation, in *Proceedings of HB2008, Nashville, TN, 2008*, pp. 75–77, https://accelconf.web.cern.ch/HB2008/papers/wga10.pdf.

[15] A. V. Fedotov *et al.*, Beam lifetime and limitations during low-energy RHIC operation, in *Proceedings of the 24th Particle Accelerator Conference, PAC-2011, New York, 2011* (IEEE, New York, 2011), pp. 2285–2287.

[16] T. Satogata, RHIC local orbit control and power supply resolution, Brookhaven National Laboratory, Upton, NY, Report No. BNL-90845-2009-TECH, 2009.

[17] A. Piwinski, Intrabeam scattering, in *Handbook of Accelerator Physics and Engineering* (World Scientific, Singapore, 1999), p. 125.

[18] The cavity frequencies are tunable so only the rounded numbers are quoted in this paper. The frequency of the 28 MHz cavities is the third harmonic of that of the 9 MHz cavities when they are used at the same time.
[19] M. Martini, Intrabeam scattering in the ACOOL-AA machines, Report No. CERN PS/84-9 (AA), 1984.
[20] A. O. Sidorin, I. N. Meshkov, I. A. Seleznev, A. V. Smirnov, E. M. Syresin, and G. V. Trubnikov, BETACOOL program for simulation of beam dynamics in storage rings, Nucl. Instrum. Methods Phys. Res., Sect. A **558**, 325 (2006).
[21] A. V. Fedotov *et al.*, Accelerator physics design requirements and challenges of RF based electron cooler LEReC, in *Proceedings of NAPAC'16, Chicago, IL, 2016* (JACoW, Geneva, Switzerland), pp. 867–869.
[22] A. V. Fedotov *et al.*, Experimental Demonstration of Hadron Beam Cooling Using Radio-Frequency Accelerated Electron Bunches, Phys. Rev. Lett. **124**, 084801 (2020).
[23] V. V. Parkhomchuk and A. N. Skrinskiĭ, Electron cooling: 35 years of development, Phys. Usp. **43**, 433 (2000).
[24] S. Nagaitsev *et al.*, Experimental Demonstration of Relativistic Electron Cooling, Phys. Rev. Lett. **96**, 044801 (2006).
[25] M. Steck, P. Beller, K. Beckert, B. Franzke, and F. Nolden, Electron cooling experiments at the ESR, Nucl. Instrum. Methods Phys. Res., Sect. A **532**, 357 (2004).
[26] A. V. Fedotov *et al.*, Operational electron cooling in the Relativistic Heavy Ion Collider, in *Proceedings of the 12th Particle Accelerator Conference, IPAC'21, Campinas, Brazil, 2021* (JACoW Publishing, Geneva, Switzerland), pp. 2516–2520.
[27] A. V. Fedotov *et al.*, IBS for RHIC operation below transition energy and various RF systems, Brookhaven National Laboratory, Upton, NY, Report No. BNL-99841-2013-IR, 2013.
[28] C. Liu *et al.*, IBS simulation with different RF configurations in RHIC, Brookhaven National Laboratory, Upton, NY, Report No. BNL-113205-2016-IR, 2016.
[29] D. Kayran *et al.*, High-brightness electron beams for linac-based bunched beam electron cooling, Phys. Rev. Accel. Beams **23**, 021003 (2020).
[30] P. R. Cameron *et al.*, The RHIC wall current monitor system, in *Proceedings of the 1999 Particle Accelerator Conference, PAC-1999, Batavia, IL, 1999* (IEEE, New York, 1999), pp. 2146–2148.
[31] T. Tsang, S. Bellavia, R. Connolly, D. Gassner, Y. Makdisi, T. Russo, P. Thieberger, D. Trbojevic, and A. Zelenski, Optical beam profile monitor and residual gas fluorescence at the relativistic heavy ion collider polarized hydrogen jet, Rev. Sci. Instrum. **79**, 105103 (2008).
[32] S. Seletskiy *et al.*, Obtaining transverse cooling with nonmagnetized electron beam, Phys. Rev. Accel. Beams **23**, 110101 (2020).
[33] S. Seletskiy *et al.*, Accurate setting of electron energy for demonstration of first hadron beam cooling with rf-accelerated electron bunches, Phys. Rev. Accel. Beams **22**, 111004 (2019).
[34] S. Seletskiy, M. Blaskiewicz, A. Fedotov, D. Kayran, and J. Kewisch, Effect of beam-beam kick on electron beam quality in first bunched electron cooler, J. Phys. Conf. Ser. **1350**, 012134 (2019).
[35] The fractional part of betatron tunes for beams in the RHIC Blue and Yellow rings is slightly different for beam control purposes. The fractional tunes in the horizontal plane are slightly higher than the ones in the vertical plane to stay below the betatron coupling resonance. Only the rounded value for the fractional part of betatron tunes is presented in this paper.
[36] J. G. Alessi *et al.*, High-performance EBIS for RHIC, in *Proceedings of the 22nd Particle Accelerator Conference, PAC-2007, Albuquerque, NM* (IEEE, New York, 2007), pp. 3782–3785.
[37] D. B. Steski *et al.*, Upgrade and operation of the BNL Tandems for RHIC injection, in *Proceedings of the Particle Accelerator Conference, Chicago, IL, 2001* (IEEE, New York, 2001), pp. 2545–2547, 2001.
[38] H. Zhao *et al.*, Cooling simulation and experimental benchmarking for an rf-based electron cooler, Phys. Rev. Accel. Beams **23**, 074201 (2020).
[39] K. Schindl, Space charge, CERN accelerator school Intermediate Course on Accelerators, Report No. CERN-2006-002, 2006.
[40] C. Montag and A. V. Fedotov, Beam-beam effects in space charge dominated ion beams, arXiv:1410.4076.
[41] J. P. Delahaye *et al.*, Shaping of proton distribution for raising the space-charge of the CERN PS Booster, Experientia **40**, 299 (1980).
[42] L. J. Laslett, V. K. Neil, and A. M. Sessler, Transverse resistive instabilities of intense coasting beams in particle accelerators, Rev. Sci. Instrum. **36**, 436 (1965).
[43] M. Blaskiewicz *et al.*, Collective Instabilities in RHIC, Brookhaven National Laboratory, Upton, NY, Report No. BNL-102147-2013-IR, 1994.
[44] G. W. Foster *et al.*, Bunch-by-bunch digital dampers for the Fermilab main injector and recycler, in *Proceedings of the 2003 Particle Accelerator Conference, Portland, OR* (IEEE, New York, 2003), pp. 323–325.
[45] N. Mounet, The LHC transverse coupled-bunch instability, Ph.D. thesis, École polytechnique fédérale de Lausanne (EPFL), 2012, 10.5075/epfl-thesis-5305.
[46] J. Bengtsson and J. Irwin, Analytical calculation of smear and tune shift, Technical Report No. SSC-232, SSC, 1990.
[47] F. Schmidt, SODD: A computer code to calculate detuning and distortion function terms in first and second order, Technical Report No. CERN SL/Note 99-009 (AP), CERN, 1999.
[48] T. Roser, Recursive transverse damping algorithms, AGS/AD Technical Note Report No. 398, 1994.
[49] F. J. Cullinan, R. Nagaoka, G. Skripka, and P. F. Tavares, Transverse coupled-bunch instability thresholds in the presence of a harmonic-cavity-flattened RF potential, Phys. Rev. Accel. Beams **19**, 124401 (2016).
[50] A. Jain, Dynamic effects in superconducting magnets, USPAS school, Phoenix, 2006.
[51] D. A. Finley *et al.*, Time dependent chromaticity changes in the Tevatron, in *Proceedings of the 1987 Particle Accelerator Conference* (IEEE, Washington, DC, 1987), pp. 151–153.

[52] F. Willeke and F. Zimmermann, The impact of persistent current field errors on the stability of the proton beam in the HERA proton ring, in *Proceedings of the 1991 Particle Accelerator Conference, San Francisco, CA, 1991* (IEEE, New York, 1991), pp. 2483–2485.

[53] D. A. Herrup, W. Kinney, M. J. Lamm, and A. Mokhtarani, Compensation of time-dependent persistent current effects in superconducting synchrotrons, Phys. Rev. E **49**, 5660 (1994).

[54] B. J. Holzer, Impact of persistent currents on accelerator performance, Part. Accel. **55**, 215 (1996).

[55] C. Montag, Multipole error data analysis for RHIC low-energy operations, Brookhaven National Laboratory, Upton, NY, Report No. BNL-99566-2013-IR, 2011.

[56] V. N. Litvinenko and D. S. Yaroslav, Coherent Electron Cooling, Phys. Rev. Lett. **102**, 114801 (2009).

[57] V. N. Litvinenko, Coherent electron cooling (CeC) experiment at RHIC: Status and plans, Brookhaven National Laboratory, Upton, NY, Report No. BNL-209778-2019-COPA, 2019.

[58] C. Liu, D. Bruno, A. Marusic, M. Minty, P. Thieberger, and X. Wang, Mitigation of persistent current effects in the RHIC superconducting magnets, Phys. Rev. Accel. Beams **22**, 111003 (2019).

[59] G. Robert-Demolaize *et al.*, Commissioning of a β^* knob for dynamic IR correction at RHIC, Brookhaven National Laboratory, Upton, NY, Report No. BNL-96720-2012-CP, 2012.

[60] C. Liu, Vertex distribution with 9 MHz cavities and comparison of 9 MHz versus 28 MHz cavities for 7.3 GeV operation, Report No. BNL-209167-2018-TECH, Brookhaven National Laboratory, Upton, NY, 2018.

[61] K. Zeno, The 2020 Low Energy Gold Run in the injectors, Brookhaven National Laboratory, Upton, NY, Report No. BNL-220777-2021-TECH, 2020.

[62] H. Huang *et al.*, Small longitudinal emittance setup in injectors with gold beam for Beam Energy Scan in RHIC, in *Proceedings of the 12th International Particle Accelerator Conference, IPAC-21, Campinas, Brazil, 2021* (JACoW Publishing, Geneva, Switzerland), pp. 90–92.

[63] P. Thieberger *et al.*, Improved gold ion stripping at 0.1 and 10 GeV/nucleon for the Relativistic Heavy Ion Collider, Phys. Rev. Accel. Beams **11**, 011001 (2008).

[64] W. Zhang, W. Fischer, H. Hahn, C. Pai, J. Sandberg, and J. E. Tuozzolo, Research and development toward the RHIC injection kicker upgrade, in *Proceedings of the 24th Particle Accelerator Conference, PAC-2011, New York, 2011* (IEEE, New York, 2011), pp. 1211-1213, https://accelconf.web.cern.ch/pac2011/papers/tup213.pdf.

[65] V. Schoefer *et al.*, RHIC injection kicker measurement and emittance growth simulation, Brookhaven National Laboratory, Upton, NY, Report No. BNL-207810-2018-TECH, 2018.